Damping and electromechanical behavior of ionic-modified brominated poly(isobutylene-co-isoprene) rubber (BIIR) containing petroleum resin C5

Xiao Hu,[a, b] Runan Zhang,[c] Alan M. Wemyss,[a] Aihua Du,[d] Xujin Bao,[e] Xueyu Geng,[b] Chaoying Wan[a*]

[a] International Institute for Nanocomposites Manufacturing (IINM), WMG, University of Warwick, CV4 7AL, UK

[b] School of Engineering, University of Warwick, CV4 7AL, UK

[c] Department of Mechanical Engineering, University of Bath, BA2 7AY, UK

[d] Key Lab of Rubber-Plastics, Ministry of Education, Qingdao University of Science and Technology, 266042, China

[e] Department of Materials, Loughborough University, LE11 3TU, UK

[*]Email: chaoying.wan@warwick.ac.uk

Abstract: To improve the damping properties of rubbers, organic tackifiers such as hydrocarbon resins, rosin esters or polyterpenes are often incorporated to increase the intermolecular friction of the rubber, thus increasing the energy dissipation (damping) during dynamic loading. However, this is often at the expense of crosslinking density and mechanical properties of the rubbers. Ionic crosslinks introduce unique properties to rubbers, such as a combination of mechanical reinforcement and high extensibility, as well as self-healing and damping, thanks to the reversible ionic association. Hence creating an ionic network would be an interesting alternative to adding small molecular tackifiers to rubbers. While the reversible ionic association inevitably causes structural instability over time (i.e., creep) or at elevated temperatures (ionic transition generally happens at 60 ~ 80 °C). To balance the dynamic damping, viscoelasticity and mechanical stability of these materials, we prepared 1-vinyl imidazole modified brominated poly(isobutylene-*co*-isoprene) (BIIR) elastomers by solid-state rubber compounding and curing processes, investigated the effects of ionic networks and an aliphatic petroleum resin (C5) on the viscoelastic and electromechanical properties of the ionic-crosslinked elastomers. We found that the mechanical reinforcement can be achieved simultaneously with a broad effective damping temperature range through optimising the ionic network and C5 concentrations. The polar ionic clusters also increased the dielectric permittivity while maintaining a low dielectric loss of the elastomers, the ionic modified BIIR exhibited similar actuation and energy harvesting properties as commercial VHB-4910 elastomer under similar configurations, which provides alternative dielectric elastomers with reprocessibility for vibration and energy harvesting applications.

Keywords: elastomers, ionic clusters, viscoelasticity, damping, energy harvesting

1. Introduction

Vibration and noise management have been long-term concerns in the transportation and manufacturing industries, as they effect operational safety and cause environmental pollution. The sources of mechanical vibration and acoustic noise range from the macroscale dynamic operation among the structural components to the microscale molecular friction of the materials. The ubiquitous vibrational energy can be dissipated and absorbed as waste-heat by damping rubbers,[1] whilst it can also be transformed into useful electrical energy by electromechanical energy transducers or thermoelectric devices.[2-4]

Elastomeric composites have been widely applied as both damping materials and flexible energy generators, thanks to their unique viscoelastic properties, low cost, easy of modification and manufacturing. However, damping performance and energy harvesting efficiency require conflicting dynamic mechanical properties of rubbers. The former requires higher mechanical hysteresis for higher energy dissipation; the latter prefers low hysteresis, fast response and higher dielectric permittivity. To select the right rubber composites for the targeted application, it is a prerequisite to understand the relationship between the crosslinked network properties and the viscoelasticity of the rubbers and their composites.

Rubber composites are able to absorb or dissipate mechanical energy through internal heat built-up, which depends on the intermolecular, filler-filler and filler-polymer friction. The energy dissipation can be determined by the mechanical loss factor ($\tan\delta$), which is the ratio of the loss modulus (E'') and storage modulus (E'), as measured by dynamic mechanical thermal analysis (DMTA). The maximum $\tan\delta$ ($\tan\delta_{max}$) value of polymers occurs at the glass transition region where the free volume of the polymers expands, accompanied by polymer chain segment

vibrations, which dissipates energy. The temperature range (ΔT) for effective damping performance is defined as the range of temperatures where tanδ > 0.3.[5]

On the other hand, most elastomers have dielectric permittivity (ε_r) of 2 ~ 4. To enhance energy conversion efficiency of elastomer-based energy generators, a higher dielectric permittivity, a lower dielectric loss factor ($tan\delta = \frac{\varepsilon''(\omega)}{\varepsilon'(\omega)}$), and a lower hysteresis are essential, according to the Figure of Merit of energy harvesting, $FoM_{Harvesting} = \varepsilon_0 \varepsilon_r E_b^2$, where ε_0 is the permittivity of a vacuum and E_b is the breakdown strength of the elastomer.[6]

Different methods have been explored to improve either the damping or energy harvesting properties of elastomers, such as chemical modification of the polymer chains by introducing polar or bulky side groups, copolymerization, interpenetrating networks, or introducing different nanofillers.[7-9] The covalent crosslinks networks of vulcanised rubber dramatically increases the glass transition temperature (T_g) of these materials due to the constrained polymer chain mobility.[10-12] While grafted polar groups can enhance intra-, and inter-molecular interactions, thus enhancing the tanδ around the T_g.[13] Tackifiers such as hydrocarbon resins, rosin esters or polyterpenes are low molecular compounds that can increase the T_g and expand the ΔT of rubber blends. Hydrocarbon resins, such as petroleum resin C5, are typically amorphous oligomers with molecular weights in the range of 300 to 3000 g/mol and a T_g near ambient temperature, and these have shown good compatibility with a number of commercial diene rubbers.[5, 13-15] Li *et al.* found the tanδ peak of chlorinated butyl rubber (CIIR) composites shifted to a higher temperature with the addition of petroleum resin.[16] Liang *et al* investigated the damping behaviour and mechanical properties of silica-filled BIIR/BR vulcanizates, and the addition of C5 led to positive shifts of the tanδ peak and a remarkable broadening of ΔT in the range of the BIIR glass transition, with much less effect on the BR domain and almost no improvement on the compatibility between BIIR and

BR.[17] Yin *et al.* studied the damping mechanism of C5/CIIR composites through experimental and molecular dynamics simulations and proposed that C5 petroleum resin was able decrease the free volume of the composites, thus confining the local segmental motion and the Rouse modes of CIIR, and van der Waals interactions played a major role in improving the damping performance of the system.[18] Aromatic petroleum resin (C9) was also shown to significantly improve the damping performance of poly(butyl methacrylate) by positively shifting the T_g and increment of tanδ_{max} [13].

The incorporation of fillers to elastomers generally increases energy dissipation due to the destruction of the filler networks at lower strain amplitude (Payne effect) as well as the interfacial friction among the polymer chains and the filler surfaces. In the case of energy transduction using rubber composites as the flexible dielectric devices, the grafting of polar groups to the polymer backbones increases their dielectric permittivity.[9, 19] However, the introduction of dielectric or conducting fillers can also increase the dielectric permittivity, but often at the expense of reducing electric breakdown strength and flexibility due to the dispersion and interfacial defects of the polymer composites.[19]

BIIR has a high tanδ_{max}, wide ΔT, high flexibility and low elastic modulus.[17, 20] However, its damping and energy harvesting performance are limited. BIIR contains approximately 1-2 *mol*% of brominiated isoprene groups. The bromide allylic group is highly reactive to nucleophile subsititution, thus offering the opportunities for further functionalisation. Parent *et al.* investigated a range of BIIR ionomers synthesized from N-alkyl imidazole, triaryl phosphine, trialkyl amine and carboxylate nucleophiles through solution state and sovlent-free mixing approaches.[21-24] The introduction of N-alkyl imidazolium functionality to BIIR overcomes the drawback of the radical degradation of the polymer chains in the process of dicumyl peroxide (DCP) curing, in addition, it results in a hybrid crosslinking network of ionic bonding and covalent bonding, so that the

elasticity, adhesion, and antimicrobial activity of the crosslinked BIIR are enhanced.[21-23, 25] A BIIR modified with 1-vinyl imidazole was reported by Kleczek and Parent.[21] They found that the ion-pair aggregates dominated the shorter time relaxation during tensile testing or dynamic oscillatory rheology, while the covalent network confered long term stability.[21] In addition, the introduction of an aggregated ion-pair network increased the loss modulus (G''), therefore a higher energy dissipation capacity was present that benefits damping.[26] In the study of Suckow, the *E''* of N-butyl imidazole and N-hexyl imidazole modified BIIR were higher than that of sulfur-cured BIIR, indicating higher energy dissipation capability.[27] However, the role of ionic clusters on the actuation and energy harvesting properties of the ionic-modified BIIR is not yet clear. How the dynamic ionic associations in the networks and the presence of C5 would benefit damping, and how they will affect the energy harvesting efficiency is unknown.

In this work, we introduce ionic clusters to BIIR through nucleophilic substitution with 1-vinyl imidazole during the compounding and curing process. C5 was added as a processing additive. The effects of ionic crosslinking and C5 concentration on the ionic-transition temperature, damping performance, mechanical and dieletric properties, as well as energy harvesting properties of the modified BIIR are studied, in comparsion with tranditional sulfur cured BIIR. The BIIR exhibited tunable damping properties by varying the C5 concentration, and comparable energy harvesting performance as compared to the commercial VHB elastomer applied for energy harvesting.

2 Experimental

2.1 Materials

BIIR (X-Butyl B2030), with a Mooney viscosity (ML (1+8) 125 °C) of 32 and a bromide content of 1.523 mol% (corresponding to the mass fraction of 1.7659 wt%), was provided by Lanxess Co., Ltd. Petroleum resin C5, with the softening point of 120 °C and the number-average molecular weight (M_n) determined by Gel Permeation Chromatography (GPC) of 839 g/mol, was purchased from Shenzhen Jitian Chemical Co., Ltd. 1-Vinyl imidazole (99%) reagent grade was purchased from Sigma-Aldrich, UK. Sulfur, N-Cyclohexylbenzothiazol-2-sulphenamide (CBS) and zinc oxide (ZnO) were commercial products and used as received.

2.2 Ionic modification of BIIR and blending with C5

BIIR compounds were prepared by mixing 1-vinyl imidazole and C5 with BIIR in a HAAKE Polylab internal mixer at 60 rpm at 40 °C for 10 min. The molar amount of 1-vinyl imidazole used was 1.65-fold excess to the alkyl bromide group of BIIR for an optimized ionic conversion[28]. The compounds were compression-moulded into sheets with dimensions of 100 × 100 × 1 mm^3 under 10 MPa. The resultant samples are denoted as BV/C5-*x*, where *x* = 10~40 phr refers the concentration of C5.

Sulfur-cured BIIR/C5 (BS/C5-*x*) were prepared for comparison, with formulation (phr) of BIIR 100, sulfur 1, stearic acid 2, zinc oxide 5, CBS 1, and C5 (0, 20 and 40) phr. The compounds were cured under 10 MPa at 160 °C for 30 mins.

2.3 Characterization

Curing tests were carried out using an Montech MDR rheometer with electrically heated base plate and electrically heated hood with the frequency of 1.77 Hz and the amplitude of 1° according to ISO 6502-1:2018 with uncompressed compounds.

Tensile tests of the compressed specimens were conducted using a Shimadzu Autograph AGS-X tester with the extension speed of 500 mm/min at room temperature according to ASTM-D638-

14 type V. To obtain stable mechanical properties, samples were kept at the room temperature for 3 days after compression processing.

Cyclic stress test was carried out for 5 cycles and for each cycle the clamped specimen was stretched to the state with the elongation of 500% and then retracted to its original position under a controlled extension rate of 100 mm/min without intervals. The hysteresis loss ratio between two different hysteresis loops can be calculated according to eq. (1),

$$H_i = \frac{LA_i}{A_i} \quad (1)$$

Where H_i, A_i and LA_i are hysteresis loss ratio, the area under the uploading stress – strain curve, and the area of the loop curve respectively for the i_{th} cycle.

Crosslinking densities of BV and BS samples were determined using an equilibrium swelling method[29]. Samples were swollen in toluene at 21 °C for 72 h to reach an equilibrium swelling state, and then dried in vacuum at 50 °C for 48 h until reached constant weights. The crosslinking density (V_e) of sulfur cured BIIR (BS) and the gross crosslinking density (V_e) involving both ionic crosslinks and covalent crosslinks of 1-vinyl imidazole modified BIIR (BV) were calculated following eq. (2) and (3). To distinguish the ionic crosslinks from covalent crosslinks, a second swelling test were conducted with BV samples. The dried BV samples were soaked in toluene and trifluoroacetic acid for 120 h to disassociate the ionic bonding, followed by drying to constant weight. As a result, the covalent crosslinking density (V_{cov}) of BV could be obtained from the second swelling test, and the ionic crosslinking density (V_{ion}) is the difference between the gross crosslinking density and the covalent crosslinking density.

$$V_r = \frac{m_0 \cdot \varphi \cdot (1-\alpha) \cdot \rho_r^{-1}}{m_0 \cdot \varphi \cdot (1-\alpha) \cdot \rho_r^{-1} + (m_1 - m_2) \cdot \rho_s^{-1}} \quad (2)$$

$$V_e = -\frac{\ln(1-V_r) + V_r + \chi V_r^2}{V_s(\sqrt[3]{V_r} - V_r/2)} \quad (3)$$

Where V_r is the volume fraction of the rubber, m_0 is the sample mass before swelling, m_1 and m_2 are the swelled sample masses before and after drying, respectively, φ is the mass fraction of polymer in the sample, α is the mass loss ratio of the polymer during swelling, and ρ_r and ρ_s are the rubber density and the solvent density; V_s is the molar volume of the solvent and χ is the polymer-solvent interaction parameter.

Dynamic mechanical thermal analysis (DMTA) was conducted using samples with size of 10 × 3.18 × 1.00 mm in tension mode, under frequency of 1Hz and the amplitude of 0.05 mm, between -65 °C and 120 °C. Impedance spectroscopy was applied to determine the dielectric properties using the Princeton Applied Research Parastat MC between 100 and 10^6 Hz.

2.4 Actuation and Energy harvesting using a conical dielectric elastomer (DE) device

With compliant electrodes applied on both faces of a thin elastomer membrane, the sandwiched structure acts as a soft capacitor. The electro-mechanical properties of the elastomer can be therefore exploited to convert electrical energy to mechanical energy, and vice versa.

In actuation, a sandwiched elastomer structure, pre-stretched and fixed on rigid frames, can be used as a force actuator. By switching on and off the driving voltage in kV, the induced electrostatic forces cause the elastomer to generate net forces, F_a, at the boundary, which correlates to the applied electrical field, Φ, as $F_a \propto \Phi^2$, where $\Phi = \frac{V}{h}\lambda_s$, with V and h being the driving voltage and the thickness of the elastomer membrane and λ_s being the areal stretch of the electrode region. Because the actuation force output of the DE actuator is linear to the square of the applied electrical field, the frequency responses of the elastomer actuator, $f(s)$, can therefore be characterized as $f(s) = \frac{F_a(s)}{\Phi^2(s)}$.

In energy harvesting, a cyclic mechanical loading (e.g. compression in thickness direction, or expansion in planar directions) stretches a elastomer and causes changes on the electrode region

(A), and thickness of the elastomer membrane (h), which correspond to the change in capacitance of the DE, $C = \varepsilon_r \varepsilon_0 \frac{A}{d}$, where ε_r is the permittivity of the elastomer, ε_0 is the permittivity of free space. When stretched, the increased capacitance allows the elastomer energy generator to drawing more electrical charges from the power source; when released, the decreased capacitance forces the drawn electrical charges to boost to higher voltages before being discharged, converting mechanical energy input to electrical energy output.

To evaluate energy harvesting performances, the mechanical energy input, W_M, is calculated as $W_M = \int F(t)\, dl(t)$, where $F(t)$ and $l(t)$ are the force and the displacement of the elastomer structure under mechanical loading. The generated electrical energy, W_E, is calculated as $W_E = \int \Phi(t)\, dQ(t)$, with $\Phi(t)$ and $Q(t)$ being the electrical field and the electrical charges on the electrode region. The energy conversion efficiency of the elastomer energy generator can therefore be expressed as $\eta = \frac{W_E}{W_M} \times 100\%$.

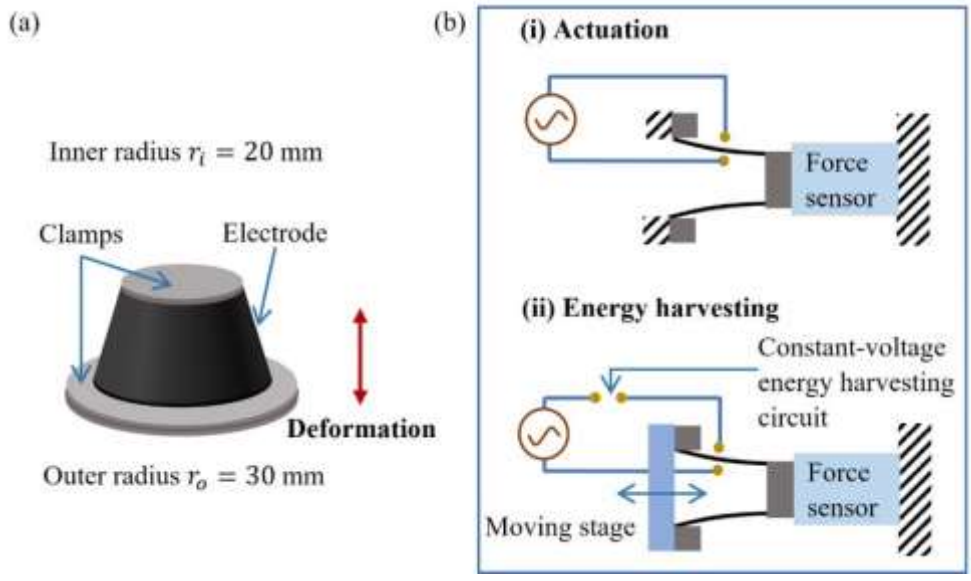

Figure 1. (a) Configuration of the conical elastomer device, and (b) schematic diagram of dual-mode operation: (i) actuator mode and (ii) energy generator mode.

Table 1. Three sets of experiments for demonstrating elastomer actuation and energy harvesting

Test No.	Description	Material candidates
1	Constant-voltage actuation	BS, BV
2	Frequency response characterisation in actuation	BS, BS/C5-40, BV and BV/C5-40
3	Constant-voltage energy harvesting	BS, BV

To demonstrate the electromechanical properties of the BV, BV/C5 composite, the BS and BS/C5 composite, three sets of experiments were conducted, as listed in Table 1, to demonstrate actuation and energy harvesting in a conical elastomer structure (see Figure 1). At each test, a thin membrane ($\sim 350\ \mu$m in thickness) was clamped with two sets of rigid frames, namely the inner and outer ring frames. A circular electrode region, with an inner radius $r_i = 20$ mm and an outer radius $r_o = 30$ mm, was formed on the membrane using carbon black grease (from MG Chemicals™). The sandwiched elastomer structure was mounted on a linear stage driven by a stepper motor and was stretched in the direction of thickness (see Figure S1). The inner ring frame is stationary and fixed on a sensor that takes force measurements; the outer ring frame is mounted on the moving stage. The areal stretch of the electrode region at each stroke l is calculated as

$$\lambda_s = \frac{(\pi r_o + \pi r_i)\sqrt{(r_o - r_i)^2 + l^2}}{(r_o^2 - r_i^2)\pi} \quad (4)$$

Note that λ_s in equation (4) only serves as a conservative estimation of the overall deformation of the electrode region. The actual deformation of a conical elastomer structure is inhomogeneous and a more accurate calculation of areal strains requires a sophisticated material model [30].

Constant-voltage elastomer actuation was demonstrated in Test 1. The BS and the BV were pre-stretched at the stroke of $l = 20$ mm and was connected directly to the high voltage power supply. Constant driving voltages were applied in steps, increasing from 0 kV to the point when electrical

breakdown occurs. Test 2 was designed to characterise frequency responses of the materials over the frequency range of 0.25-20 Hz. The BS, the BS/C5-40, the BV and the BV/C5-40 were tested under the same pre-strain as in Test 1. A chirp signal (1~3 kV) was used to excite elastomer actuators over 20 seconds. For each material, the frequency response was evaluated using equation (5-6) between the force output and the actual voltage output of the power source, rather than the demand voltage signal to exclude dynamics of the power source.

In Test 3, energy harvesting processes were demonstrated in conical energy generator, using the BS and BV. A constant-voltage energy harvesting circuit shown in Figure S2 was used in this test. The voltage input is set to be 1.5 kV (i.e. $\Phi_L = 1.5$ kV). Diode D2 is an assembly of Zener diodes in series to establish a constant harvesting voltage of 2 kV (i.e. $\Phi_H = 2$ kV). Diode D1 blocks the discharged current flow from the DE structure to the power source. To exclude dissipation of electrical charges in the circuit and through the DE due to defects, it is assumed that there is no loss of charges during the process (i.e. $Q_L = Q_H$) and electrical energy is always harvested at Φ_H. Over each energy harvesting cycle, the sandwiched elastomer structure stretched and released at a constant speed of 10 mm/s, with no pause in between to minimize the effect of relaxation on the processes. At each stroke, the loading cycle was repeated 5 times and the energy harvesting performance is evaluated using only the last cycle, when the stress-strain behavior becomes stable. For each material, the energy harvesting test was conducted with the stroke starting from $l = 10$ mm, at an increment of 10 mm, to the point when electrical breakdown occurs.

3 Results and discussion

3.1 Curing characteristics of BV/C5 compounds

During the curing process, 1-vinyl imidazole displaces the allylic bromide group of BIIR via nucleophilic substitution and forms vinyl imidazolium/bromide ion pairs, which tend to aggregate and act as ionic crosslinks in the elastomer. Meanwhile, there is a possibility of polymerisation initiated by macroradicals incurred by the bromide leaving group in BIIR backbone, as shown in Figure 2(a). As a result, we synopsized that a hybrid network comprised of ionic associations and covalent crosslinks was formed in the 1-vinyl imidazole modified BIIR (BV), which is different from the covalent network of conventionally cured BIIR (BS).

The curing behaviour of BV and BS between 100 and 160 °C are shown in Figure 2 (b) to (d). In Figure 2 (b), the BV exhibits an obvious marching modulus at 100 °C. After the torque rapidly increased during the first 2 min, it then increased almost linearly with the curing time. At 140 °C and 160 °C, the torque climbed more rapidly within a short period, followed by a moderate progression, which could be attributed to the oligomerization of excessive 1-vinyl imidazole or the covalent reaction between 1-vinyl imidazole and BIIR. The t_{90} of BV was measured to be 36.5 min at 140 °C, and after addition of 20 and 40 phr C5, the t_{90} was 37.5 and 40 min, respectively. The torque of BV and BS decreased dramatically with the addition of C5 due to the low viscosity of C5 at elevated temperature, see Figure 2 (c). The conventional BS formulation was cured at 160 °C, and the t_{90} of BS, BS/C5-20, BS/C5-40 was measured to be 43.9, 32.0 and 23.1 mins, respectively. Based on the curing behavior of BV and BV/C5 blends, the condition for compounding in this study was set as 140 °C for 30 min. The curing process of BS and BS/C5 blends followed the conventional condition of 160 °C for 30 min.

BV was found to swell in toluene and tetrahydrofuran (THF) solvents, and the mass of the swelled part became less once several drops of acetic acid were added to the solvent and leave the sample for 120 h, which verified that the existence of the hybrid network. The crosslinking density

of BV and BS blends was investigated, the covalent crosslinking of BV was distinguished from the hybrid crosslinking by breaking ionic aggregations with acetic acid in the swelling test. As it was shown in Figure 2 (d), the gross crosslinking density of BV (V_e = 8.9 ×10^{-4} mol/cm^3) is measured to be half of that of BS and the ionic crosslinking density (V_{ion}) of BV comprises 46.1% of the V_e. The existence of ionic clusters will probably benefit the mechanical properties of modified BIIR according to the reference[32]. The V_e of both BV/C5 and BS/C5 constantly decreased with the increasing of C5, and the decreasing ratio was 66.2% and 77.5% respectively with 40 phr C5 added into BV and BS, as well as the V_{ion} of BV, which can be attributed to the dilution effect of C5 on the concentration of crosslinking system. Additionally, part of crosslinkers and accelerators were possibly included in C5, and thus isolated from BIIR backbone, resulting in the inhibition to crosslinking process.

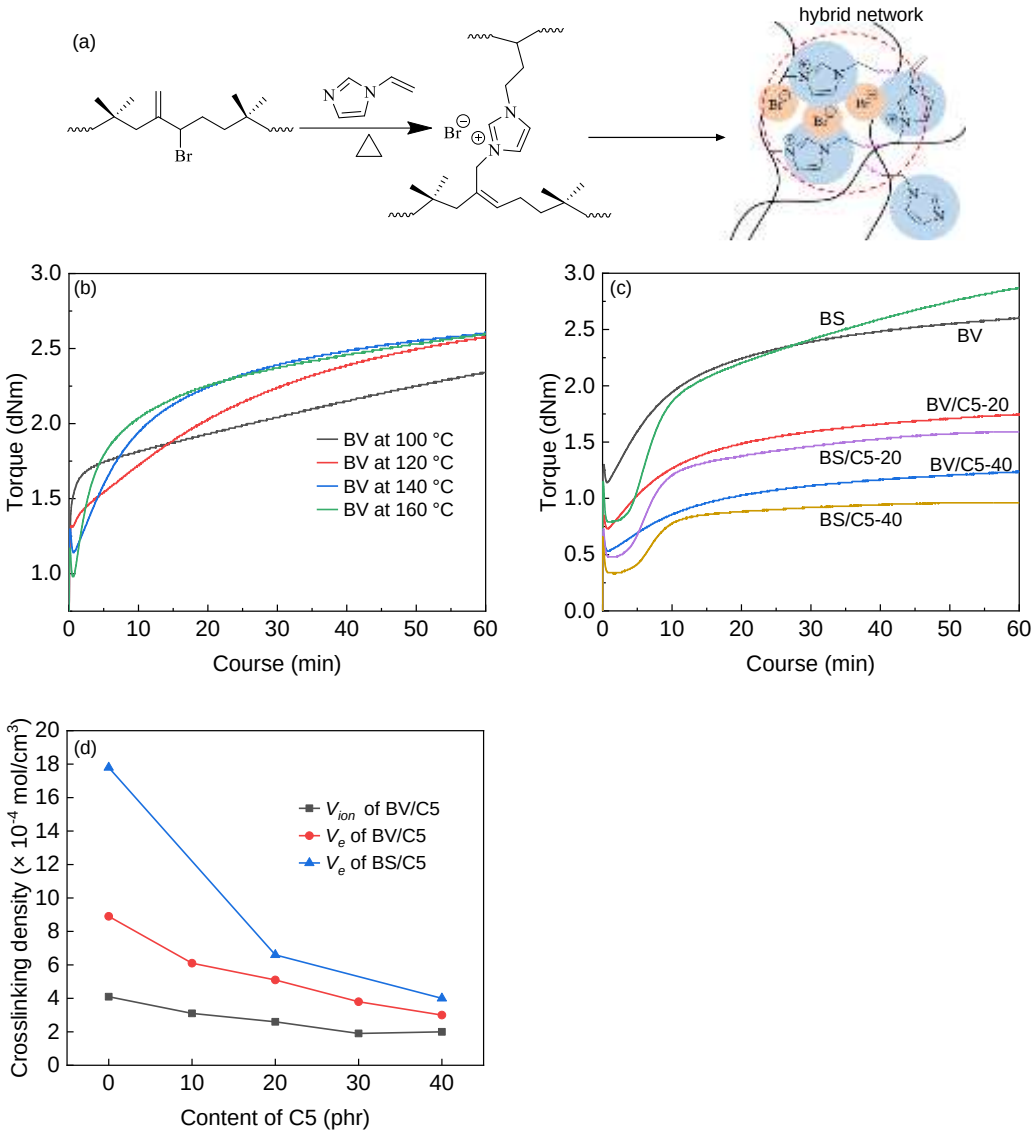

Figure 2. (a) The schematic of nucleophile displacement and crosslinking reaction between 1-vinyl imidazole and BIIR, (b) Curing curve analysis of BV at various temperatures, (c) Curing curves of BS containing different contents of C5 at 160 °C, (d) Crosslinking density of BV/C5 (cured at 140 °C for 30min) and BS/C5 (cured at 160 °C for 30min) blends.

3.2 Mechanical and damping properties

The combination of ionic associations and covalent crosslinks may benefit both the mechanical strength and extensibility of the elastomers, as well as damping properties due to the reversible association/disassociation of ionic interactions. The ionically modified BIIR (BV) shows a tensile strength of 15.0 ± 1.9 MPa, 20% higher than the sulfur-cured BIIR (BS) as shown in Figure 3 (a) and (b), despite the much lower gross crosslinking density of BV compared to BS. The elongation at break of BV was 1552 ± 195%, which is slighter lower than was observed in BS.

Figure 3 (c) shows the creep behavior of BV and BS at room temperature under constant stress of 2.0 MPa. The strain of BS remained at about 785% while the strain of BV kept growing and increased by 165% of its original value after 90 mins. The extended strain of BV can be ascribed to the continuous breakdown and slippage of the ionic aggregates under the constant stress, which is a common observation in polymer networks that are crosslinked with dynamic bonds.[6] The BS is permanently covalently crosslinked and relatively stable.

With the addition of 10 to 40 phr C5, the tensile strength of BV decreased by 29.3% and the elongation at break increased by 10.4%, as shown in Figure 3(d). In comparison, the addition of 40 phr C5 significantly reduced the tensile strength of BS by 50% and increased the elongation at break by 32.0%. The inclusion of the C5 resin decreased the crosslinking concentration and hindered the crosslinking reaction and thus reduced the crosslink density of both BV and BS (Figure 3(b)), which fits well the result of Figure 2 (d).

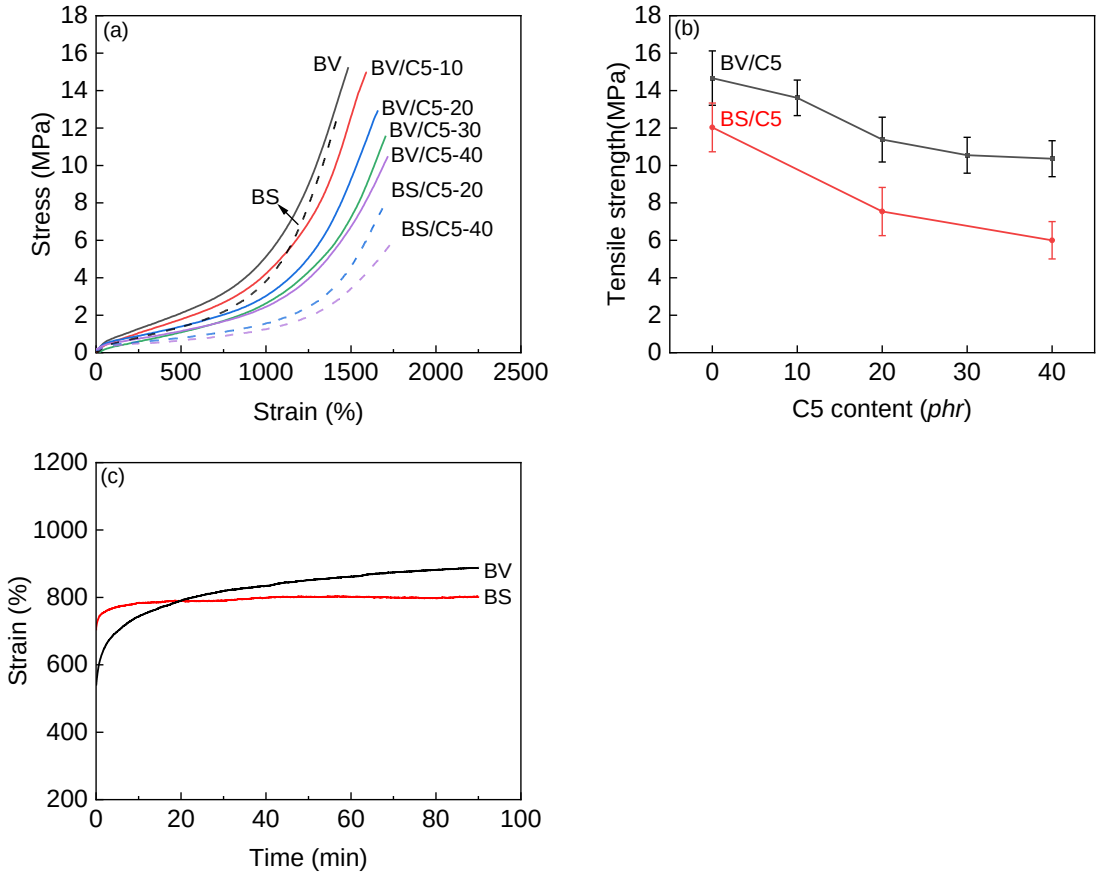

Figure 3 (a) Stress - strain curve of BV/C5 and BS/C5 blends, (b) Tensile strength of BV/C5 and BS/C5 blends with different C5 contents, (c) Creep behavior of BV and BS under constant stress of 2.0 MPa.

The mechanical hysteresis was evaluated by cyclic tensile testing, the results of BV/C5 and BS/C5 blends with different C5 contents are shown in Figure 4 and Figure S3. Over five cycles under a strain of 500%, all the samples exhibited typical stress-softening with permanent residual strain. The area under the uploading curve and the hysteresis loop area presents the input energy and the energy dissipated during the cycle. The input energy and the hysteresis loop of BV and BV/C5 composites was higher than the BS and BS/C5 composite for each cycle. This is attributed

329 to the molecular interactions being enhanced by the ionic aggregates, of which the deformation
330 and breakdown dissipates more mechanical energy. Dramatic hysteresis loss ratio decreases were
331 observed for both BV/C5 and BS/C5 composites after the first cycle with insignificant variation
332 for the following four cycles. Although the addition of C5 decreased the hysteresis loop area of all
333 blends, the different effect of various dosages of C5 on hysteresis loss ratio of BV and BV/C5
334 blends was not obvious. After five cycles, the hysteresis loss ratio for BV and BV/C5 blends was
335 0.2 (Figure 4 (e)). With respect to BS and BS/C5 blends, the addition of C5 produced a higher
336 hysteresis loss ratio for each cycle, which indicated that C5 molecular chains were involved in the
337 energy dissipation during the cyclic test.

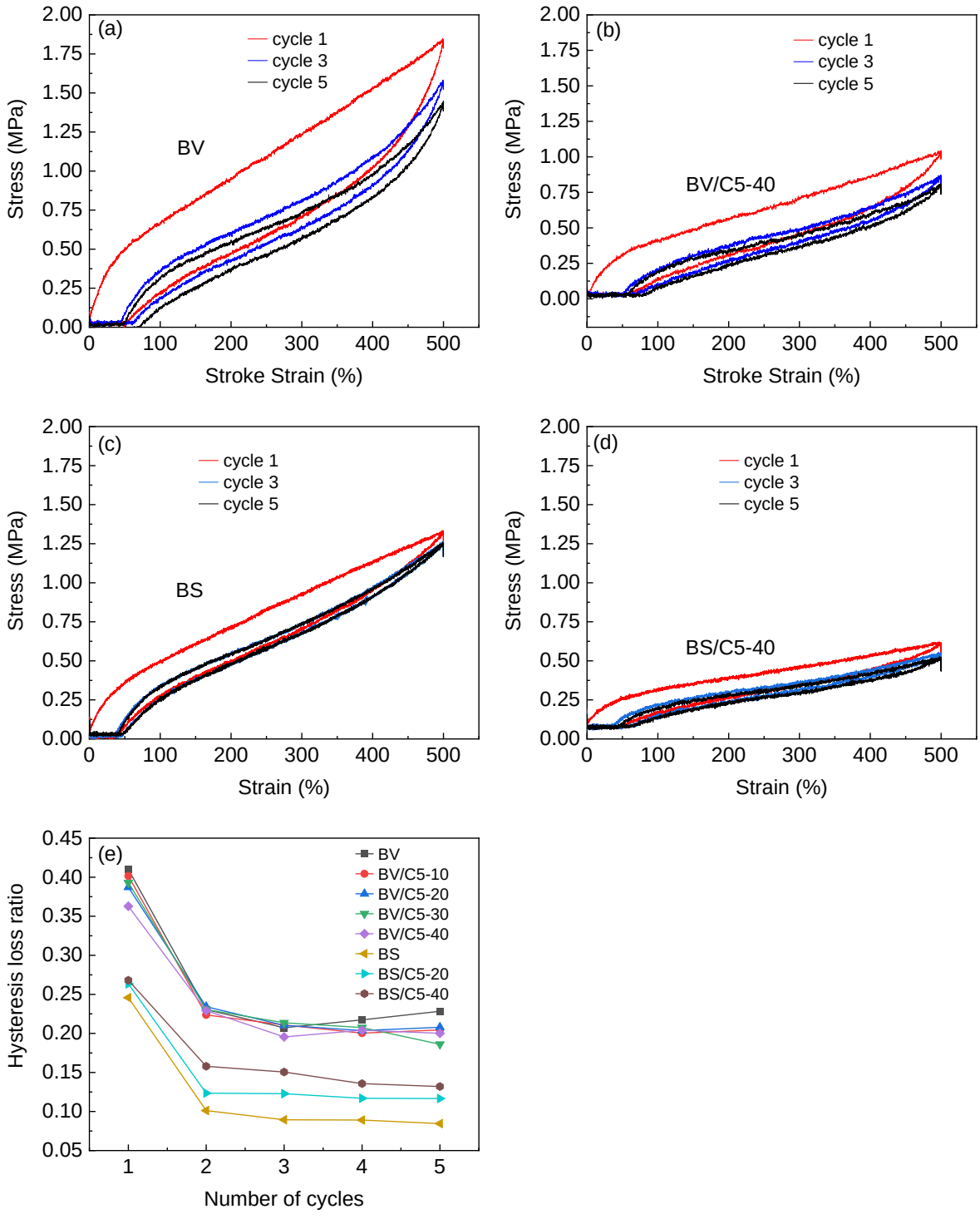

338

339 Figure 4. Cyclic test result of (a) BV, (b) BV/C5-40, (c) BS and (d) BS/C5-40, and (e) hysteresis

340 loss ratio of BV/C5 and BS/C5 blends.

The dynamic damping properties of the modified BIIR are evaluated using DMTA. The maximum tanδ value (tanδ_{max}) of polymers occurs at their glass transition region, where their free volume expands and the molecular chain segments vibrate, thus dissipating energy. A broader ΔT that covers the working temperature of the materials and a higher tanδ_{max} value benefit damping performance.[5, 33] As shown in Figure 5 (a), an asymmetric peak below 0 °C with a shoulder on the lower temperature side was observed for the BV samples containing different C5 contents, and an additional relaxation peak varying between 60 and 80 °C were observed. The temperature corresponding to tanδ_{max} (T_{peak}) of BV and BS (Figure 5 (a) and (b)) was located at around -34 °C with only slight difference in the value of tanδ_{max}, which was determined by the restriction of crosslinking network on the chain mobility. Compared to BS, BV containing hybrid crosslinks showed the higher E' (Figure 5 (c)), corresponding to higher mechanical reinforcement. BV and BV/C5 composites had a distinct relaxation in the E'' plateau region in Figure 5 (d), which highlighted the hysteresis mechanism as the structural rearrangement of ionic aggregates.[34-36] However, the tanδ value of peaks related to the rearrangement of ionic clusters were lower than 0.3 (Figure 5(a)) as a consequence of less energy being consumed in this process.

The addition of C5 shifted the T_{peak} of BV and BS from below 0 °C to higher temperatures with slightly reduced peak height (Figure 5 (a). It was worth noting that by increasing the amount of C5 from 0 to 40 phr in BV the tanδ peak at low temperature increased by 23.5 °C without huge value loss, while the shoulder stayed at the same temperature at around -52 °C accompanied a considerable tanδ loss of 0.6. The distance between the tanδ peak and the sub-Rouse mode shoulder was extended, possibly because the distributed C5 resin molecules fill the free volume of BV and thus retard the Rouse mode with long chains, leading to much higher internal friction, while the sub-Rouse mode that involves less carbons was only slightly influenced due to the smaller size.[37]

We calculated the activation energy (E_a) needed to mobilise one mole of rubber chains to quantify the internal friction within BV/C5 and BS/C5 composites by using the Arrhenius-type equation:[38]

$$\frac{E\prime}{E_0} = exp\left[\frac{E_a}{R}\left(\frac{1}{T} - \frac{1}{T_0}\right)\right] \quad (5)$$

where E' and E_0 are the storage modulus at temperature T and at the reference temperature T_0 respectively, and R is the universal gas constant, 8.31 J/(K·mol). As shown in Figure 5 (f) and (g), log E' is almost linear to the inverse temperature, and as a result, E_a is proportional to the slope of the line.

As shown in Table 2, the E_a of the BIIR chains kept growing with increasing C5 amount, indicating the higher energy required to overcome the internal friction for mobilizing one mole of BIIR chains, and with the same content of C5, the BS/C5 composites consumed more energy to overcome this mobility restriction. Slight negative shifts were observed in the ionic bond related peaks with the addition of C5, possibly because the electrostatic interactions and inter/intra-molecular force among ionic clusters were weakened and less energy were required for the rearrangement. Both BS/C5-40 and BV/C5-40 presented a broad tanδ curve which centered near -10 °C with the desirable ΔT of 99.5 °C and 81.1 °C respectively, meeting many engineering service temperature demands.

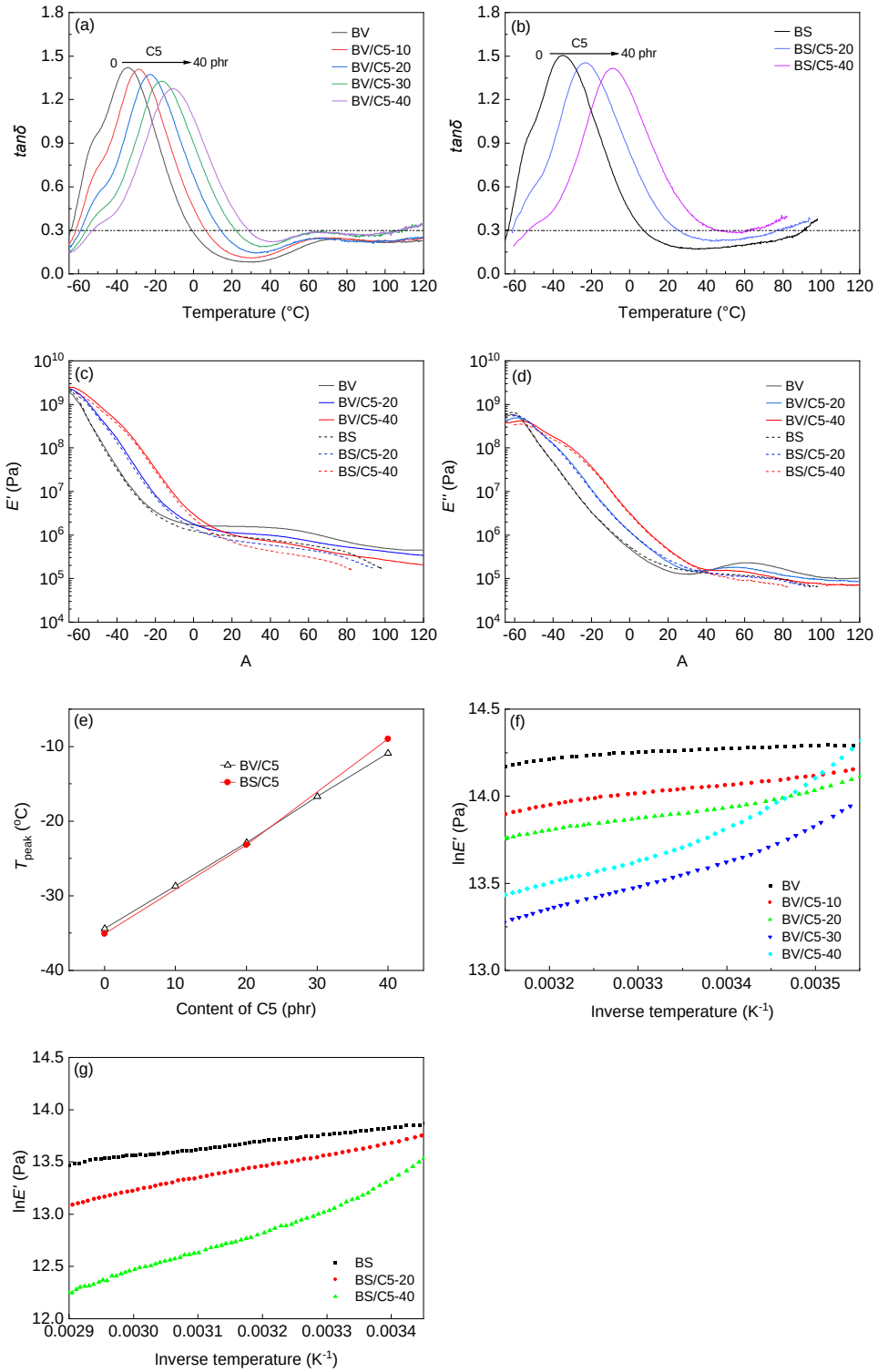

382

383 Figure 5. (a) tanδ vs temperature curve of BV and BV/C5 composites, (b) tanδ vs temperature

384 curve of BS and BS/C5 composites, (c) *E'* vs temperature curve of BIIR composites, (d) *E''* vs

temperature curve of BIIR composites, (e) T_{peak} vs C5 content of BIIR composites, (f) lnE' vs inverse temperature of BV and BV/C5 composites, and (g) lnE' vs inverse temperature of BV and BV/C5 composites.

Table 2. DMTA Parameters of BV and BS samples

Mass ratios of C5/BIIR	$\tan\delta_{max}$		$\tan\delta > 0.3$			
	Value	T_{peak}(°C)	T_1^a	T_2^a	ΔT (°C)	E_a (kJ/mol)
BV/C5-0	1.42	-34.4	-64.0	0.9	64.9	2.24
BV/C5-10	1.41	-29.1	-61.4	6.4	67.8	4.84
BV/C5-20	1.37	-22.9	-58.6	14.0	72.6	6.44
BV/C5-30	1.33	-16.7	-51.6	21.9	73.5	13.26
BV/C5-40	1.28	-10.9	-52.6	28.5	81.1	16.69
BS	1.50	-35.1	-64.3	5.6	67.2	6.79
BS/C5-20	1.45	-23.2	-61.2	31.1	92.3	11.75
BS/C5-40	1.42	-9.0	-52.7	46.8	99.5	22.42

[a]T_1 and T_2 are the minimum value and maximum temperature value of the constant curve interval corresponding to $\tan\delta > 0.3$, respectively.

3.3 Actuation and energy harvesting of ionic modified BIIR

Figure 6 (a) to (d) displays the relative permittivity (ε_r), AC conductivity, phase angle and dielectric loss of BV, BS and BV/C5-40 as a function of frequency. It is found that the introduction of ionic clusters led to the higher relative permittivity of BV and BV/C5 between 3.0 and 3.5 compared to the BS of 2.86 (at 1000 Hz), which can be ascribed to the polarity of the immobilised ionic clusters. The relative permittivity, phase angle and dielectric loss of BV and BS were frequency-independent at the range of 10^2 to 10^5 Hz, however, with the addition of C5, the BV/C5

and BS/C5 composites were subject to dramatic dielectric loss beyond 10^3 Hz, especially BS/C5-20.

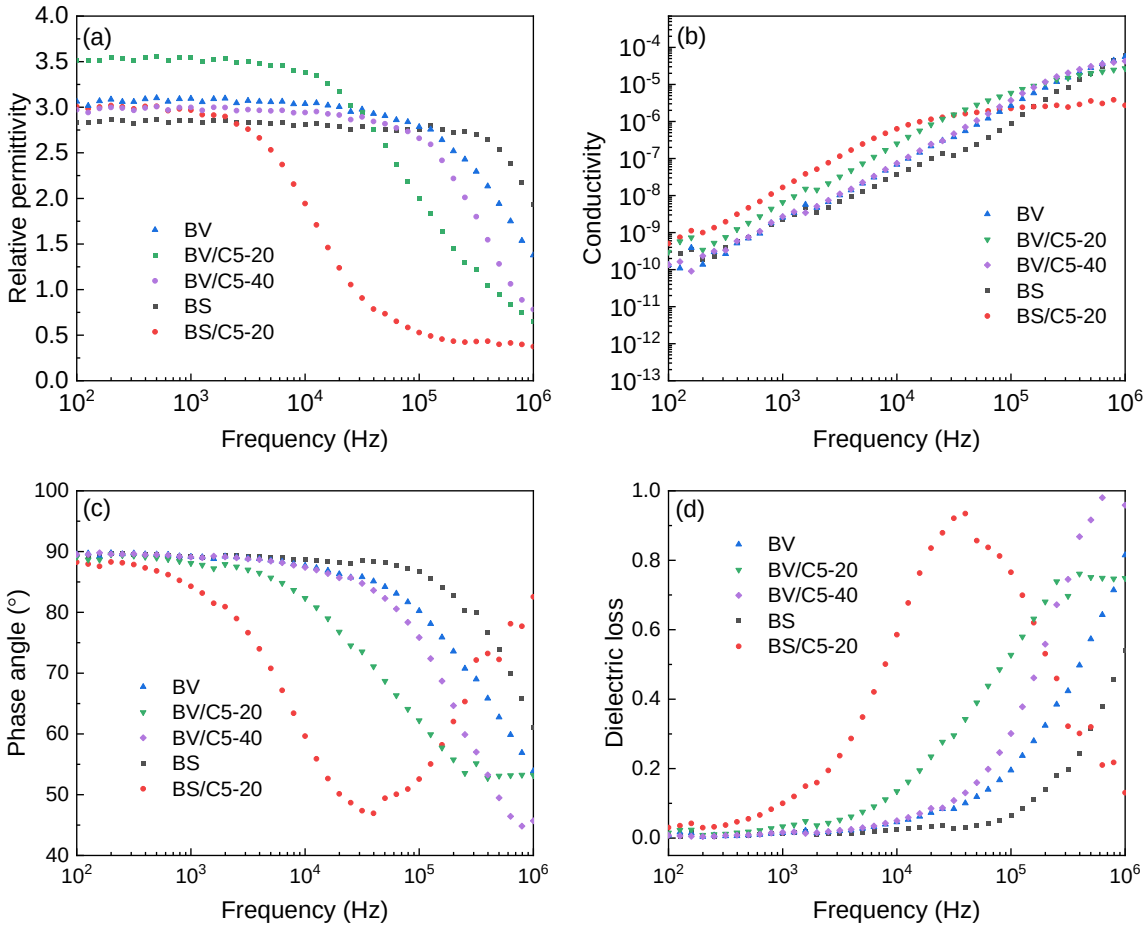

Figure 6. The frequency dependence of (a) relative permittivity; (b) AC conductivity; (c) Phase angle and (d) dielectric loss of BV, BS and BV/C5

Figure 7 (a) shows the steady-state force outputs of the BS and the BV-based DE actuators and showed that at the steady state (i.e. at 0 Hz), BV and BS had similar actuation force outputs at up to 30 MVm^{-1}. BV generated a maximum force of 2N at a maximum electrical field of 47 MVm^{-1}. BS generated a maximum force of 0.44 N at a maximum electrical field of 30 MVm^{-1}. In comparison, the BV was comparable to the commercial VHB-4910 elastomer, the commonly used

polyacrylate, which generates a maximum force output of 1.7 N in a similar configuration of conical DE actuator.[30]

Figure 7 (b) compares the frequency responses of BV, BV/C5-40, BS and BS/C5-40 from actuation tests. The results represented how responsive each dielectric elastomer actuator was under electrical stimulation at different frequencies. The frequency responses of BV/C5-40, BS and BS/C5-40 were similar throughout the frequency range of 0.25~20 Hz, and all four materials shared similar responses at frequencies up to 1 Hz. The BV became less responsive at higher frequencies (>1 Hz). At 20 Hz, the frequency response of the BV was 50% lower than that of the other 3 materials (i.e. 0.5×10^{-3} Nm^2/MV^2 compared with 1×10^{-3} Nm^2/MV^2), meaning that the actuation force output of the BV would be only half of the other 3 materials under the same electrical stimulation at 20 Hz.

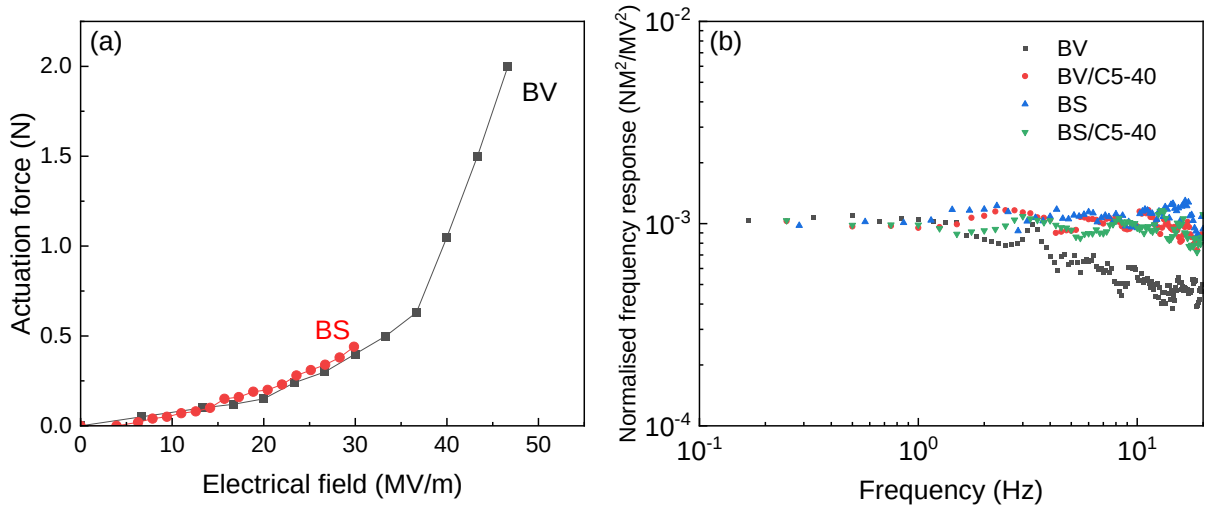

Figure 7. (a) Steady-state force outputs of the BS and the BV-based DE actuators (i.e. at 0 Hz), and (b) Frequency responses of the BV, BV/C5-40, BS and BS/C5-40 based actuators over the frequency range of 0.25-20 Hz (for comparison, all results are normalized in relative to the response of the BV at 0 Hz).

Table 3. Energy harvesting results of the BS and BV-based energy generators.

Stroke l (mm)	Areal strain λ_s (%)	BV			BS		
		W_M (mJ)	W_E (mJ)	η (%)	W_M (mJ)	W_E (mJ)	η (%)
10	140	0.4	-	0	-	-	0
20	220	5	-	0	14	-	0
30	320	37	0.5	1.35	35	0.6	1.85
40	410	85	1.2	1.41	62	1.1	1.78
50	510	150	1.8	1.20	99	1.7	1.69

Table 3 shows the results of BS and BV in energy harvesting tests. At each stroke, l, and the areal strain, λ_s, was calculated using equation (5); the mechanical and the electrical energy, W_M and W_E, and the energy conversion efficiency, η, was calculated using equations presented in the Experimental 2.4. For both materials, electrical breakdown occurred at the stroke of 60 mm and the corresponding electrical field at breakdown was 26 MVm^{-1}. Compared with the actuation results, BS and BV energy generators failed at a lower electrical field due to defects and stress concentration at larger deformation (stroke > 20 mm). The energy conversion efficiency peaks at 1.41% at the stroke of 40 mm for BV, and at 1.85% at the stroke of 30 mm for the BS. As the stroke increased further, the energy conversion efficiency started to decline due to a combination of material stiffening, relaxation, and deterioration in electrode coverage. Compared with BV, BS generated the same amount of electrical energy from less mechanical energy (i.e. 99 mJ compared with 150 mJ at the stroke of 50 mm) due to reduced damping. As a result, the energy conversion efficiency of BS is higher than that of BV even though their dielectric properties were similar. It was also observed that the energy harvesting cycles at low strokes of 10 mm and 20 mm were heavily affected by relaxation, resulting extremely low electrical energy output. At the stroke of 50 mm, the maximum electrical energy outputs of BS and BV were 1.8 mJ and 1.7 mJ, corresponding to a similar maximum energy density of 3.4 mJ/g (i.e. the density of BS and BV

were measured to be 0.96 g/cm^3, and the total mass of the electrode region was 0.53 g). Overall, the energy harvesting performances of BS and BV were comparable to the polyacrylate VHB 4905 without pre-strain, which has an energy conversion efficiency below 2% and an energy density below 2 mJ/g under similar configurations. [39]

The energy harvesting experiments demonstrate that as an alternative to increasing dielectric and breakdown strengths of a dielectric elastomer, the energy conversion efficiency can be improved by reducing energy dissipation due to its viscoelastic behavior. Hence, tuning mechanical properties of dielectric elastomers can also have significant effects in optimizing their energy harvesting performances.

4. Conclusions

1-vinyl imidazole modified BIIR (BV) was prepared via solid-state rubber compounding and curing processes. The ionic clusters combined with the covalent crosslinks in the modified BIIR exhibited a higher reinforcement effect than conventionally sulfur vulcanized BIIR (BS), although with a higher creep behavior. The addition of C5 to BV decreased the mechanical properties but improved the damping properties. BV/C5-40 showed a wide ΔT of 81.1 °C, from -52.6 and 28.5 °C, and a high $\tan\delta_{max}$ of 1.28. With the same C5 content, BV/C5 retained higher mechanical properties compared with the BS/C5 composites, while the damping properties of BS/C5 composites were improved more than the BV/C5 composites.

Overall, the ionic crosslinks enhanced the mechanical properties and relative permittivity of BIIR. The BV generated a maximum force of 2 N at a maximum electrical field of 47 MVm^{-1} at 0 Hz, while the higher frequency response of BV is not as improved as sulfur-cured BIIR. The energy conversion efficiency peaks of BV was 1.41% at a stroke of 40 mm, and its maximum electrical

468 energy outputs was 1.7 mJ, which is comparable to the energy harvesting of commercial VHB-
469 4910 elastomer.
470
471 ASSOCIATED CONTENT
472 Supporting Information: Figures of energy harvesting at constant-voltage and cyclic test result
473 of BV/C5-10, BV/C5-20, BV/C5-30 and BS/C5-20
474 Author Contributions
475 The manuscript was written through contributions of all authors. All authors have given approval
476 to the final version of the manuscript.
477
478 ACKNOWLEDGMENT
479 C.W. thanks for the support of RSC International Exchange Scheme (IEC\NSFC\191291).
480 ABBREVIATIONS
481 BIIR, brominated poly(isobutylene-*co*-isoprene); BV, 1-vinyl imidazole modificed BIIR; BS,
482 sulfur cured BIIR; C5, aliphatic petroleum resin; BV/C5-*x*, the blends of BV and *x* (= 10~40 phr)
483 of C5; BS/C5-*x*, the blends of BS and *x* (= 10~40 phr) of C5.
484 **References**
485 (1) Fan, R.; Meng, G.; Yang, J.; He, C. Experimental study of the effect of viscoelastic damping
486 materials on noise and vibration reduction within railway vehicles. *Journal of Sound and Vibration*
487 **2009**, *319*, 58-76. DOI: 10.1016/j.jsv.2008.03.071.
488 (2) Hosseinkhani, A.; Younesian, D.; Eghbali, P.; Moayedizadeh, A.; Fassih, A. Sound and
489 vibration energy harvesting for railway applications: A review on linear and nonlinear techniques.
490 *Energy Reports* **2021**, *7*, 852-874. DOI: 10.1016/j.egyr.2021.01.087.
491 (3) Shen, H.; Qiu, J.; Balsi, M. Vibration damping as a result of piezoelectric energy harvesting.
492 *Sensors and Actuators A: Physical* **2011**, *169* (1), 178-186. DOI:
493 https://doi.org/10.1016/j.sna.2011.04.043.

(4) Tianchen, Y.; Jian, Y.; Ruigang, S.; Xiaowei, L. Vibration energy harvesting system for railroad safety based on running vehicles. *Smart Materials and Structures* **2014**, *23* (12). DOI: 10.1088/0964-1726/23/12/125046.
(5) Liu, K.; Lv, Q.; Hua, J. Study on damping properties of HVBR/EVM blends prepared by in situ polymerization. *Polymer Testing* **2017**, *60* (2017), 321-325. DOI: 10.1016/j.polymertesting.2017.02.026.
(6) Wemyss, A. M.; Ellingford, C.; Morishita, Y.; Bowen, C.; Wan, C. Dynamic Polymer Networks: A New Avenue towards Sustainable and Advanced Soft Machines. *Angewandte Chemie International Edition* **2021**, *60* (25), 13725-13736. DOI: https://doi.org/10.1002/anie.202013254.
(7) Ellingford, C.; Wemyss, A. M.; Zhang, R.; Prokes, I.; Pickford, T.; Bowen, C.; Coveney, V. A.; Wan, C. Understanding the enhancement and temperature-dependency of the self-healing and electromechanical properties of dielectric elastomers containing mixed pendant polar groups. *Journal of Materials Chemistry C* **2020**. DOI: 10.1039/d0tc00509f.
(8) Ellingford, C.; Pengchaicharoen, A.; Wemyss, A. Structure and Dielectric Properties of Electroactive Tetraaniline Grafted Non-Polar Elastomers. *Journal of Composites Science* **2020**, *4*, 25. DOI: 10.3390/jcs4010025.
(9) Ellingford, C.; Bowen, C.; McNally, T.; Wan, C. Intrinsically Tuning the Electromechanical Properties of Elastomeric Dielectrics: A Chemistry Perspective. *Macromol Rapid Commun* **2018**, *39* (18), e1800340. DOI: 10.1002/marc.201800340.
(10) Wu, J.; Huang, G.; Pan, Q.; Zheng, J.; Zhu, Y.; Wang, B. An investigation on the molecular mobility through the glass transition of chlorinated butyl rubber. *Polymer* **2007**, *48* (26), 7653-7659. DOI: 10.1016/j.polymer.2007.11.006.
(11) Bandzierz, K.; Reuvekamp, L.; Dryzek, J.; Dierkes, W.; Blume, A.; Bielinski, D. Influence of Network Structure on Glass Transition Temperature of Elastomers. *Materials (Basel)* **2016**, *9* (7). DOI: 10.3390/ma9070607.
(12) Wemyss, A. M.; Bowen, C.; Plesse, C.; Vancaeyzeele, C.; Nguyen, G. T. M.; Vidal, F.; Wan, C. Dynamic crosslinked rubbers for a green future: A material perspective. *Materials Science and Engineering: R: Reports* **2020**, *141*. DOI: 10.1016/j.mser.2020.100561.
(13) Wan, S.; Zhou, S.; Huang, X.; Chen, S.; Cai, S.; He, X.; Zhang, R. Effect of Aromatic Petroleum Resin on Damping Properties of Polybutyl Methacrylate. *Polymers (Basel)* **2020**, *12* (3). DOI: 10.3390/polym12030543.
(14) Shi, X.; Li, Q.; Fu, G.; Jia, L. The effects of a polyol on the damping properties of EVM/PLA blends. *Polymer Testing* **2014**, *33*, 1-6. DOI: 10.1016/j.polymertesting.2013.10.007.
(15) Zhang, F.; He, G.; Xu, K.; Wu, H.; Guo, S.; Zhang, C. Damping mechanism and different modes of molecular motion through the glass transition of chlorinated butyl rubber and petroleum resin blends. *Journal of Applied Polymer Science* **2014**, *131* (13), n/a-n/a. DOI: 10.1002/app.40464.
(16) Li, C.; Wu, G.; Xiao, F.; Wu, C. Damping behavior of sandwich beam laminated with CIIR/petroleum resins blends by DMA measurement. *Journal of Applied Polymer Science* **2007**, *106* (4), 2472-2478. DOI: 10.1002/app.25450.
(17) Liang, J.; Chang, S.; Feng, N. Effect of C5 petroleum resin content on damping behavior, morphology, and mechanical properties of BIIR/BR vulcanizates. *Journal of Applied Polymer Science* **2013**, *130* (1), 510-515. DOI: 10.1002/app.39202.
(18) Yin, C.; Zhao, X.; Zhu, J.; Hu, H.; Song, M.; Wu, S. Experimental and molecular dynamics simulation study on the damping mechanism of C5 petroleum resin/chlorinated butyl rubber

composites. *Journal of Materials Science* **2018**, *54* (5), 3960-3974. DOI: 10.1007/s10853-018-3134-2.
(19) Christopher, E.; Zhang, R.; Wemyssc, A. M.; Bowenb, C.; McNallya, T.; Figiela, Ł.; Wan, C. Intrinsic tuning of styrene-butadiene-styrene (SBS) based self-healing dielectric elastomer actuators with enhanced electromechanical properties. *ACS Applied Materials & Interfaces* **2020**, *8* (22), 6167-6173.
(20) Rwawiire, S.; Tomkova, B.; Militky, J.; Hes, L.; Kale, B. M. Acoustic and thermal properties of a cellulose nonwoven natural fabric (barkcloth). *Applied Acoustics* **2017**, *116*, 177-183. DOI: 10.1016/j.apacoust.2016.09.027.
(21) Kleczek, M. R.; Whitney, R. A.; Daugulis, A. J.; Parent, J. S. Synthesis and characterization of thermoset imidazolium bromide ionomers. *Reactive and Functional Polymers* **2016**, *106*, 69-75. DOI: 10.1016/j.reactfunctpolym.2016.07.019.
(22) Xiao, S.; Parent, J. S.; Whitney, R. A.; Knight, L. K. Synthesis and characterization of poly(isobutylene-co-isoprene)-derived macro-monomers. *Journal of Polymer Science Part A: Polymer Chemistry* **2010**, *48* (21), 4691-4696. DOI: 10.1002/pola.24256.
(23) Parent, J. S.; Penciu, A.; Sergio A. Guille´n-Castellanos; Andrea Liskova, a. R. A. W. Synthesis and Characterization of Isobutylene-Based Ammonium and Phosphonium Bromide Ionomers. *MAcromolecules* **2004**, *37*, 7477-7483.
(24) Parent, J. S.; Porter, A. M. J.; Kleczek, M. R.; Whitney, R. A. Imidazolium bromide derivatives of poly(isobutylene-co-isoprene): A new class of elastomeric ionomers. *Polymer* **2011**, *52* (24), 5410-5418. DOI: 10.1016/j.polymer.2011.10.021.
(25) Dakin, J. M.; Shanmugam, K. V. S.; Twigg, C.; Whitney, R. A.; Parent, J. S. Isobutylene-rich macromonomers: Dynamics and yields of peroxide-initiated crosslinking. *Journal of Polymer Science Part A: Polymer Chemistry* **2015**, *53* (1), 123-132. DOI: 10.1002/pola.27462.
(26) Ozvald, A.; Scott Parent, J.; Whitney, R. A. Hybrid ionic/covalent polymer networks derived from functional imidazolium ionomers. *Journal of Polymer Science Part A: Polymer Chemistry* **2013**, *51* (11), 2438-2444. DOI: 10.1002/pola.26629.
(27) Suckow, M.; Mordvinkin, A.; Roy, M.; Singha, N. K.; Heinrich, G.; Voit, B.; Saalwächter, K.; Böhme, F. Tuning the properties and self-healing behavior of ionically modified poly(isobutylene-co-isoprene) rubber. *Macromolecules* **2017**, *51* (2), 468-479. DOI: 10.1021/acs.macromol.7b02287.
(28) Das, A.; Sallat, A.; Bohme, F.; Suckow, M.; Basu, D.; Wiessner, S.; Stockelhuber, K. W.; Voit, B.; Heinrich, G. Ionic modification turns commercial rubber into a self-healing material. *ACS Appl Mater Interfaces* **2015**, *7* (37), 20623-20630. DOI: 10.1021/acsami.5b05041.
(29) Liu, Y.; Li, Z.; Liu, R.; Liang, Z.; Yang, J.; Zhang, R.; Zhou, Z.; Nie, Y. Design of Self-Healing Rubber by Introducing Ionic Interaction To Construct a Network Composed of Ionic and Covalent Cross-Linking. *Industrial & Engineering Chemistry Research* **2019**, *58* (32), 14848-14858. DOI: 10.1021/acs.iecr.9b02972.
(30) Wang, H. M.; Zhu, J. Y.; Ye, K. B. Simulation, experimental evaluation and performance improvement of a cone dielectric elastomer actuator. *Journal of Zhejiang University: Science A* **2009**, *10* (9), 1296-1304, Article. DOI: 10.1631/jzus.A0820666 Scopus.
(31) Lu, J.; Yan, F.; Texter, J. Advanced applications of ionic liquids in polymer science. *Progress in Polymer Science* **2009**, *34* (5), 431-448. DOI: 10.1016/j.progpolymsci.2008.12.001.
(32) Das, A.; Sallat, A.; Bohme, F.; Sarlin, E.; Vuorinen, J.; Vennemann, N.; Heinrich, G.; Stockelhuber, K. W. Temperature scanning stress relaxation of an autonomous self-healing

elastomer containing non-covalent reversible network junctions. *Polymers (Basel)* **2018**, *10* (1). DOI: 10.3390/polym10010094.
(33) Qin, R.; Huang, R.; Lu, X. Use of gradient laminating to prepare NR/ENR composites with excellent damping performance. *Materials & Design* **2018**, *149*, 43-50. DOI: 10.1016/j.matdes.2018.03.063.
(34) Huang, J.; Zhang, L.; Tang, Z.; Guo, B. Bioinspired engineering of sacrificial bonds into rubber networks towards high-performance and functional elastomers. *Composites Communications* **2018**, *8*, 65-73. DOI: 10.1016/j.coco.2017.11.002.
(35) MACKNIGHT, W. J.; EARNEST, T. R. The Structure and Properties of Ionomers. *Journal of Polymer Science: Macromolecular Reviews* **1981**, *16*, 41-122.
(36) MacKnight, W. J.; Earnest Jr., T. R. The structure and properties of ionomers. *Journal of Polymer Science: Macromolecular Reviews* **1981**, *16* (1), 41-122. DOI: https://doi.org/10.1002/pol.1981.230160102.
(37) Wu, J.; Huang, G.; Wang, X.; He, X.; Xu, B. Changes in the Viscoelastic Mechanisms of Polyisobutylene by Plasticization. *Macromolecules* **2012**, *45* (19), 8051-8057. DOI: 10.1021/ma3001274.
(38) Luo, Y.; Wang, R.; Zhao, S.; Chen, Y.; Su, H.; Zhang, L.; Chan, T. W.; Wu, S. Experimental study and molecular dynamics simulation of dynamic properties and interfacial bonding characteristics of graphene/solution-polymerized styrene-butadiene rubber composites. *RSC Advances* **2016**, *6* (63), 58077-58087, 10.1039/C6RA08417F. DOI: 10.1039/C6RA08417F.
(39) Jiang, Y.; Liu, S.; Zhong, M.; Zhang, L.; Ning, N.; Tian, M. Optimizing energy harvesting performance of cone dielectric elastomer generator based on VHB elastomer. *Nano Energy* **2020**, *71*, Article. DOI: 10.1016/j.nanoen.2020.104606 Scopus.